A Letters Journal Exploring the Frontiers of Physics

OFFPRINT

Detrended fluctuation analysis of numerical density and viscous fingering patterns

M. P. M. A. Baroni, A. De Wit and R. R. Rosa

EPL, **92** (2010) 64002

A Letters Journal Exploring the Frontiers of Physics

December 2010

EPL, **92** (2010) 64002
doi: 10.1209/0295-5075/92/64002

www.epljournal.org

Detrended fluctuation analysis of numerical density and viscous fingering patterns

M. P. M. A. Baroni[1,2], A. De Wit[2] and R. R. Rosa[1(a)]

[1] *Laboratório Associado de Computação e Matemática Aplicada, Instituto Nacional de Pesquisas Espaciais (INPE) 12201-970, São José dos Campos-SP, Brazil*
[2] *Nonlinear Physical Chemistry Unit, Faculté des Sciences, Université Libre de Bruxelles (ULB) CP 231, 1050 Brussels, Belgium, EU*

received 9 August 2010; accepted in final form 2 December 2010
published online 17 January 2011

PACS 47.11.-j – Computational methods in fluid dynamics
PACS 47.54.-r – Pattern selection; pattern formation
PACS 05.40.-a – Fluctuation phenomena, random processes, noise, and Brownian motion

Abstract – We study transversely averaged concentration profiles of fingering dynamics from numerical simulations. Such profiles are studied here for a comparative fluctuation analysis between density fingering (DF) and viscous fingering (VF) envolving in a quite similar nonlinear regime. Although many physical properties influence the fingering pattern formation in miscible displacements, there are few measurements obtained from the averaged profiles, as the mixing length, that help to characterize concentration fluctuations due to self-correlations in the interfacial structure. Besides mixing length, scaling exponents (α) from detrended fluctuation analysis (DFA) are computed here for DF and VF simulations. The scaling exponent evolution is compared between DF and VF cases providing a specific signature for each kind of process: DF with $\alpha = 1.93 \pm 0.04$ and VF with $\alpha = 1.82 \pm 0.04$. Our analysis, based on DFA, provides a new approach for quantifying the fingering pattern formation and, in particular, the fine fluctuations differences between viscous and density fingering in miscible fluids displacements.

Introduction. – Directional growth characterization has long been recognized of special interest in pattern formation theory [1,2]. A typical example may be found in the study of fingering phenomena that can occur at the interface between two fluids with different physical properties. If a less viscous fluid displaces a more viscous one in a porous medium or Hele-Shaw cell (two glass plates separated by a thin gap), then the interface deforms into fingers, hence the name *viscous fingering* (VF) [3–8]. Density fingering (DF) due to a Rayleigh-Taylor instability occurs, on the other hand, when a dense fluid lies on top of a less dense one under the gravity field influence [8–10]. These two instabilities provide similar patterns and several characteristic dynamical features such as spreading, shielding, coalescence and tip splitting, are observed in both cases. In principle, a quantitative comparison of such fingering phenomena can be provided by both linear stability analysis of relevant models [4,8,9] and numerical simulations [6,8,9]. In the linear regime, Manickam and Homsy [8] have already pointed out that dispersion curves (giving the growth rate of perturbations around the interface as a function of their wave numbers) for miscible DF and VF can be identical for a specific set of parameters values. They have furthermore discussed the conditions for which a vertical DF pattern, driven by buoyancy differences, can be analogous to a horizontal VF pattern induced by displacement at a fixed speed of one viscous fluid by a less viscous one. However, as the DF and VF dynamics follow different evolution equations it is thus expected, especially in the nonlinear regime, that some fine fluctuation differences between them should nevertheless be measurable. Hence, it is the objective of this article to perform a comparative fluctuation analysis of DF and VF simulated patterns by computing the scaling exponents from DFA (Detrended Fluctuation Analysis) [11] on transversely averaged DF and VF concentration fingering profiles. Before doing so, let us first recall classical models of DF and VF which were used to perform the respective fingering patterns simulations.

Miscible density and viscous fingering. – Our model system is a two-dimensional porous medium or thin Hele-Shaw cell of length L_x and width L_y in which two miscible solutions of different physical properties are

(a) E-mail: reinaldo.rosa@pq.cnpq.br

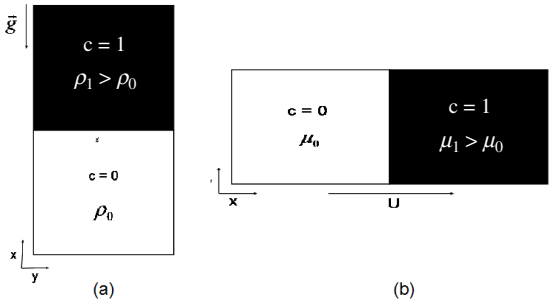

Fig. 1: Schematic of the miscible displacement process for (a) DF and (b) VF.

put in contact at $t=0$. The density or viscosity of these solutions are supposed to depend on the concentration c of a given solute. Such an initial condition can be obtained by placing in contact, at $t=0$, one solution of a solute at concentration c_1 with a solution of the same solvent where $c=0$ (see fig. 1).

The system can be described by Darcy's law for the incompressible velocity field $\underline{u}=(u,v)$ coupled to a convection-diffusion equation for the concentration c [4,5,8,10]:

$$\underline{\nabla}\cdot\underline{u}=0, \tag{1}$$

$$\underline{\nabla}p=-\frac{\mu(c)}{\kappa}\underline{u}+\rho(c)\underline{g}, \tag{2}$$

$$\frac{\partial c}{\partial t}+\underline{u}\cdot\underline{\nabla}c=D\nabla^2 c, \tag{3}$$

where the permeability κ and the diffusion coefficient D are constant, while p represents the pressure, μ the viscosity, ρ the density and $\underline{g}$ is the acceleration due to gravity.

Density fingering. To analyze fingering due to a Rayleigh-Taylor instability, we assume that the viscosity μ is constant and that only the density $\rho(c)$ is varying according to the local concentration c of the solute [10]. For dilute solutions, the density depends on c to first order of a Taylor series expansion in c as $\rho(c)=\rho_0+(\rho_1-\rho_0)\frac{c}{c_1}$, where $\rho_1=\rho(c=c_1)$ and $\rho_0=\rho(c=0)$ with $\rho_1>\rho_0$. The gravity field $\underline{g}$ is oriented downwards along x as shown on fig. 1(a) and there is no injection in the system. At initial time, a solution of c in concentration c_1 (*i.e.* of dimensionless concentration $c/c_1=1$) is put on top of another solution where $c=0$ [9].

Let us then use a characteristic geometric length h (such as the gap of a Hele-Shaw cell for instance) as characteristic length scale and define the characteristic time $\tau=h^2/D$ and speed $U=h/\tau=D/h$. The pressure, density and concentration are scaled by $\frac{\mu D}{\kappa}$, ρ_0 and c_1, respectively. The dimensionless evolution equations for density fingering become then

$$\underline{\nabla}\cdot\underline{u}=0, \tag{4}$$

$$\underline{\nabla}p=-\underline{u}+R_a\ c\ \underline{e}_x, \tag{5}$$

$$\frac{\partial c}{\partial t}+\underline{u}\cdot\underline{\nabla}c=\nabla^2 c, \tag{6}$$

where $\underline{e}_x$ is the unit vector along x, p contains now the hydrostatic pressure and the Rayleigh number R_a is defined as

$$R_a=\frac{\Delta\rho g\kappa h}{\nu D}, \tag{7}$$

where $\Delta\rho=(\rho_1-\rho_0)/\rho_0$ and $\nu=\mu/\rho_0$ is the kinematic viscosity. The dimensionless domain width and length of the system become, respectively, $L'_y=L_y/h$ and $L'_x=L_x/h$. Taking the curl of eq. (5) and introducing the stream function $\psi(x,y)$ such that $u=\frac{\partial\psi}{\partial y}$ and $v=\frac{-\partial\psi}{\partial x}$, we obtain the final dimensionless equations describing DF formation:

$$\nabla^2\psi=R_a c_y, \tag{8}$$

$$\frac{\partial c}{\partial t}+c_x\psi_y-c_y\psi_x=\nabla^2 c. \tag{9}$$

Viscous fingering. Viscous fingering occurs when a less viscous fluid of viscosity μ_0 displaces a more viscous one of viscosity $\mu_1>\mu_0$ in a porous medium at a constant speed U (see fig. 1(b)). To model such VF, here ρ is a constant and the viscosity depends on the concentration c of the solute. The constant buoyancy term is absorbed in the hydrostatic pressure. Switching to a frame moving with the injection speed U, we use now U as characteristic speed, $L_h=D/U$ and $\tau=D/U^2$ as length and time scales. Pressure, viscosity and concentration are scaled by $\mu_0 D/\kappa$, μ_0 and c_1, respectively. Dimensionless equations become

$$\underline{\nabla}\cdot\underline{u}=0, \tag{10}$$

$$\underline{\nabla}p=-\mu(\underline{u}+\underline{e}_x), \tag{11}$$

$$\frac{\partial c}{\partial t}+\underline{u}\cdot\underline{\nabla}c=\nabla^2 c. \tag{12}$$

The dimensionless viscosity is assumed to change exponentially with concentration as

$$\frac{\mathrm{d}(\ln\mu)}{\mathrm{d}c}=+R, \tag{13}$$

where $R=\ln(\mu_1/\mu_0)$ corresponds to the log-mobility ratio. VF occurs as soon as $R>0$. In terms of the stream function, the final dimensionless equations are given by [6]

$$\nabla^2\psi=-R(c_x\psi_x+c_y\psi_y+c_y), \tag{14}$$

$$\frac{\partial c}{\partial t}+c_x\psi_y-c_y\psi_x=\nabla^2 c. \tag{15}$$

Comparing the final dimensionless equations (8), (9) for DF and eqs. (14), (15) for VF, it can be seen that differences exist in the vorticity term $w(x,y)=-\nabla^2\psi$ between VF and DF, which should lead to different dynamics.

Numerical simulations. To perform our comparative analysis, we have obtained typical DF and VF evolution by direct numerical simulations for $R=R_a=3$, often investigated as a canonical unstable case [6,8,12]. The final dimensionless equations (8), (9) and (14), (15) are numerically solved using the pseudo-spectral method introduced

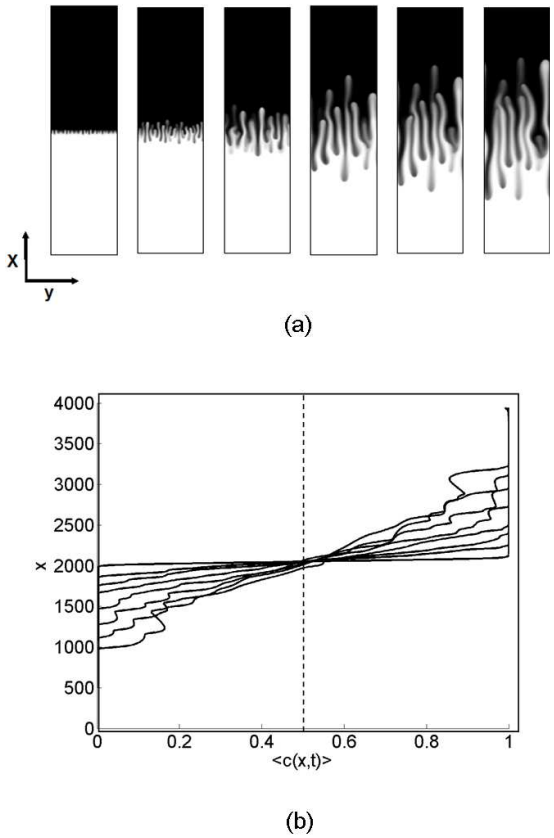

Fig. 2: (a) Evolution of DF ($t = 250$, 500, 1000, 1500, 1750, 2000) obtained from numerical integration of eqs. (8), (9) with $R_a = 3$. (b) Example of corresponding transversely averaged profiles.

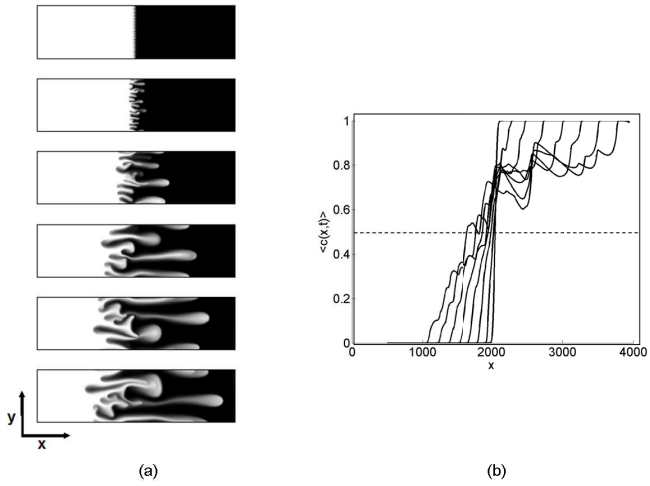

Fig. 3: (a) Evolution of VF ($t = 250$, 500, 1000, 1500, 1750, 2000) obtained from numerical integration of eqs. (14), (15) with $R = 3$. Note that, for visualization purposes, there is a long time delay between each frame so that we are missing the intermediate dynamics whereby the longer finger grows and the neigbouring ones change direction to merge with the most advanced one. (b) Example of corresponding transversely averaged profiles.

by Tan and Homsy [6]. The boundary conditions are periodic in x and y directions while the initial condition is $\psi = 0$ for all (x, y) and two back to back step functions between $c = 1$ and $c = 0$ with intermediate point where $c = 1/2 + Ar$. Here, r is a random number between 0 and 1, and A is the amplitude of the noise of order 10^{-3}. All simulations are started with exactly the same noise and performed in a typical system of length $L'_x = 4096$ and width $L'_y = 1024$. The spatial discretization uses a ratio of 4 between the number of spectral modes and the dimensionless width and length, hence the computational domain has here 1024×256 nodes. Therefore, the 1D spatial profiles that will be analyzed in the next section are discretized on 1024 points. The corresponding time step is $\mathrm{d}t = 0.2$. The dynamics of the fingering instability is computed up to a dimensionless time $t = 2000$ which allows to follow the system up to a well developed nonlinear regime for which large values of the mixing length are produced. It has been checked that the fingering dynamics remains the same with spatial and time step refinements. Examples of density and viscous fingering simulated for our comparative analysis are shown in figs. 2(a) and 3(a), respectively.

Analysis of averaged concentration profiles. – Nonlinear dynamics of VF and DF are followed by examining the evolution of 2D concentration fields $c(x, y, t)$ in the course of time, such as shown in figs. 2 and 3. At successive times, these 2D concentration fields can be spatially averaged along either the longitudinal, x, or transverse, y, coordinate to yield one-dimensional (1D) averaged profiles. The longitudinally averaged profiles $\langle c(y, t)\rangle$ provide an insight into the temporal evolution of the number of fingers, while the transversely averaged profiles $\langle c(x, t)\rangle$ feature the characteristics of the time evolution of the length of the fingering zone between two miscible solutions bringing more structural information on the mixing between the two fluids. Therefore, such transversely averaged concentration (TAC) profiles $\langle c(x, t)\rangle$ will provide the data used here for a comparative analysis between DF and VF pattern formation. The TAC profile is given by

$$\langle c(x,t)\rangle = \frac{1}{L'_y}\int_0^{L'_y} c(x,y,t)\mathrm{d}y \qquad (16)$$

and is related to standard 1D curves measured through detectors placed along porous columns, for instance [7,13]. In the absence of any fingering, such 1D profiles feature the standard error function characteristic of the time evolution of an interface between two miscible solutions when starting from an anticorrelated step function. In the presence of fingers, these transversely averaged profiles feature bumps expressing the presence of concentration fluctuations across the transverse direction along the fingers. Figures 2(b) and 3(b) show transversely averaged profiles

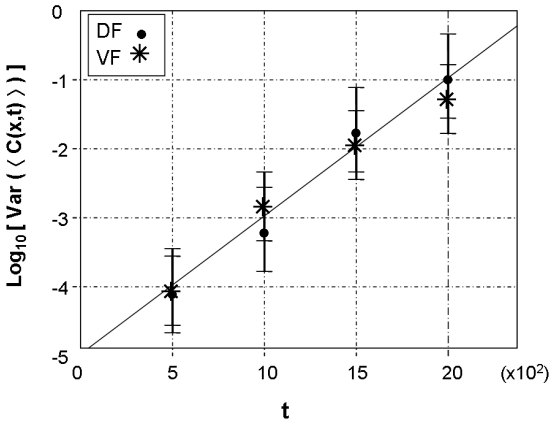

Fig. 4: Representative values of variance of $\langle c(x,t)\rangle$ for DF (dot) and VF (star) as a function of fingering evolution time. The error bars were calculated from an average over fifteen runs, for DF and VF, using different initial random seed in each simulation.

for different times in the nonlinear evolution of DF and VF patterns, respectively. Quantitatively this nonlinear spatiotemporal fingering can be characterized statistically using the variance of TAC fluctuation growth throughout time. The result is reported in fig. 4 where we depict the log of $\langle c(x,t)\rangle$ variance for four representative average snapshots ($t=500$, $t=1000$, $t=1500$ and $t=2000$) over fifteen runs of DF and VF numerical schemes. It must be noted that the linear increase of $\log_{10} Var[\langle c(x,t)\rangle]$ along time is evident from a least-square fitting and represent the typical increase of fluctuations due to the fingering pattern formation processes. It is also worth noting that the result showed in fig. 4 indicates that the fluctuations of DF and VF do not show any statistically significant difference between them. Hence to generate more detailed information about the DF and VF differences an alternative comparative analysis of typical DF and VF fingering fluctuation properties is then performed using the following structural measurements:

Mixing length. Transversely averaged profiles can be used to define the tip and rear of the fingered zone. The tip is chosen arbitrarily as the location along the x-axis in front of which the averaged concentration $\langle c(x,t)\rangle$ is larger than 0.99. The rear corresponds, on the other hand, to the location behind which $\langle c(x,t)\rangle$ is smaller than 0.01. For VF, these points represent the most and least advanced locations of the fingered zone (fig. 3). For DF, they are the highest and lowest points of the fingered zone in the gravity field, respectively (fig. 2). The mixing length, L, is defined as the distance between the tip and the rear of the fingers and gives information of the spatial extent of the mixing zone in which the two fluids are intertwined [7]. As shown in figs. 2(b) and 3(b), nonlinear fingering growth is characterized by the presence of bumps in the transversely averaged concentration profiles and an increase in the mixing length (see fig. 6(a)). However, although mixing length is commonly used to obtain such a structural signature of the fingering pattern formation it does not reveal any statistical property of fingering fluctuation.

Next we introduce the method which provides a quantitative measure of the correlation between concentration values over spatial scales along the fingering transversely averaged concentration profiles.

Detrended fluctuation analysis. DFA measures scaling exponents from non-stationary fluctuations profiles. It is useful for characterizing fluctuation patterns that appear to be due to long-range spatial or/and temporal correlations. DFA has been used in several analysis from biological and physiological data to signals in econometry and physics (*e.g.*, [14–18]).

The DFA algorithm, introduced by [14], is composed of four main computational operations starting here on a discrete series of amplitudes $\{C_i\}$:

1) *Discrete integration and windowing*: Calculate the cumulative representation of $\{C_i\}$ as $y(k)=\sum_{i=1}^{k}(C_i-\langle C\rangle)$, with $k=1,2,\ldots,N$, where $\langle C\rangle=\sum_{i=1}^{N} C$ is the average of $\{C_i\}$. Using an arbitrary local window of length n, divide $y(k)$ into non-overlapping $N_n=\mathrm{int}(N/n)$ sub-interval y_j ($j=1,2,\ldots,N_n$). Note that each sub-interval y_j has length n and N may not be the integer multiple of n. Then, the series $y(k)$ is divided once more from the opposite side to make sure all points are addressed, performing at the end of this operation $2N_n$ sub-intervals on each profile.

2) *Fitting and variance*: Get, in each sub-interval, the least-square fits $p_j^m(k)$ where m is interpreted as the *order of the detrended trend*, and compute the cumulative deviation series in every sub-interval, where the trend has been subtracted: $y_j(k)=y(k)-p_j^m(k)$. Then, calculate the variance of the $2N_n$ sub-intervals for $j=1,2,\ldots,N_n$ and $j=N_n+1,N_n+2,\ldots,2N_n$.

3) *Fluctuation*: Calculate the average of all the variances and the square root. Then get the fluctuation function $F(n)$:
$$F(n)=\left[\frac{1}{2N_n}\sum_{j=1}^{2N_n}F^2(j,n)\right]^{1/2}. \qquad (17)$$

4) *Scaling exponent*: Perform again, recursively, computation from windowing to calculation of corresponding $F(n)$ with different $n([N/4]>n=2m+2)$ box lengths. In general, in the presence of fluctuations in the form of power law: $F(n)=Kn^{\alpha}$, $F(n)$ increases linearly with increasing n. Then, using the linear least-square regression on the double-log plot, $\log F(n)=\log K+\alpha \log n$, one can get the slope α.

The slope α which is the scaling exponent of the DFA method characterizes the long-range power-law correlation

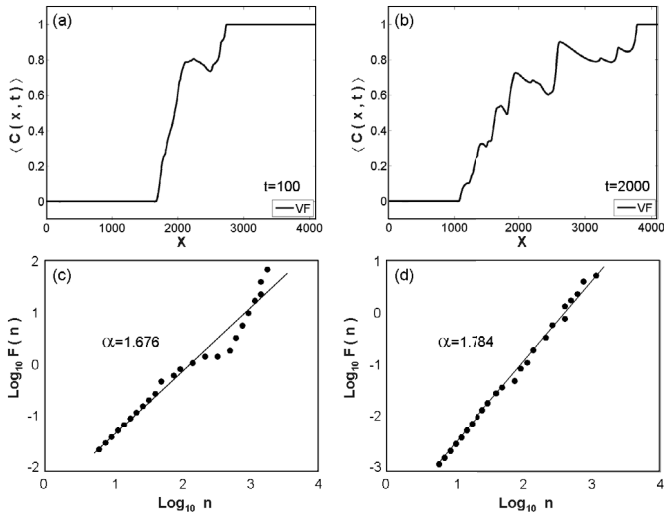

Fig. 5: Two snapshots for $t=100$ (a) and $t=2000$ (b) of transverse averaged profiles $\langle c(x,t)\rangle$ for a VF simulation with $R=3$. (c) and (d) show the respective scaling exponents computed from DFA.

properties of the fingering average profile: if $\alpha=0.5$ the fluctuations are uncorrelated and for $\alpha>0.5$ the correlation in the profile is persistent. Note that, due to the growing persistence of TAC fluctuations, here the expected values for α are always greater than 0.5. Then in the present application α works as a characteristic measure varying during the fingering evolution and its behaviour along this evolution is used to characterize the fingering pattern formation by means of the spatial correlation of average concentration profile evolving in time. Figure 5 depicts examples of two snapshots and their respective scaling exponents from DFA where we observe that the value of α increases as the spatial correlated fluctuation increases.

Let us consider, for DF and VF comparison, the respective transversely averaged profiles $\langle c(x,t)\rangle$ simulated from $t=0$ to $t=2000$. By computing the two structural measures $L(t)$ and $\alpha(t)$ for every single $\langle c(x,t)\rangle$ of the time sequence, we can characterize the DF and VF differences from the very beginning up to the final snapshot. The time ($t_{0,d}(\%)$) from where the structural differences between DF and VF was captured through each characteristic measure is given as a percentage of the whole evolution from $t=1$ (0%) to $t=2000$ (100%). The average behaviour, over fifteen runs, of each structural measure for DF and VF is shown in fig. 6 where $t_{0,d}=13.4\%$ for L and $t_{0,d}=9.6\%$ for α. Therefore, the results show that the fine differences due to the mean interface fluctuations (mixing length) start slightly later than the differences due to the long-range correlated nonlinear coarsening (scaling exponent) during the averaged concentration profile evolution. Except for the small range around $t=950$, the values of mixing length for DF are greater than the values for VF. A similar behaviour is observed for values of $\alpha(t)$ giving $\overline{\alpha}_{DF}/\overline{\alpha}_{VF}>1$ for $t>t_{0,d}$. Both

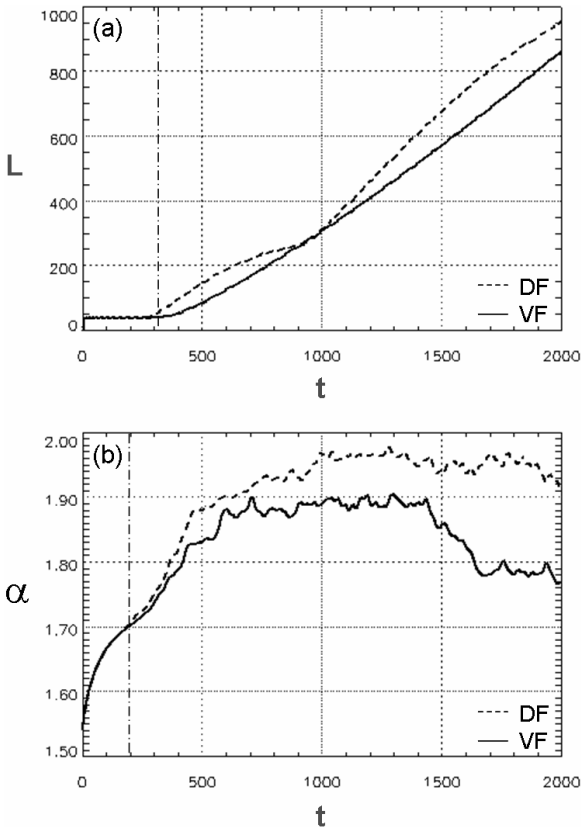

Fig. 6: Typical fluctuation measurements averaged over fifteen runs, computed for DF and VF patterns: Mixing length (a); DFA scaling exponents (b). On both figures the dash-dotted vertical line on the left indicates the time when the DF/VF difference starts, namely, $t_{0,d}$. The standard deviation of each measure, over fifteen runs, is of 2%.

measurements are showing that fluctuations due to the Rayleigh-Taylor instability (DF) are slightly stronger than those due to viscosity (VF). In fig. 6(b) we observe that the most different fingering patterns, comparing DF and VF, appear during the last 50% of the pattern formation processes after snapshot $t=1000$ having a maximum from snapshot $t=1500$ (75%) to snapshot $t=2000$ (100%).

The scaling exponent α for all simulations ($2000\times 15=30\times 10^3$ measurements for each kind of fingering: DF and VF), using a polynomial fitting of the order of 1, gave rise to the histograms showed in fig. 7. An automatic analysis of these histograms, considering a generalized extreme value distribution [19], provides the mean $\alpha_{DF}=1.93\pm 0.04$ and $\alpha_{VF}=1.82\pm 0.04$. Such scaling exponents averages on DF and VF simulations provide a new fingering pattern characterization, therefore they can play an important role in fluid fingering data analysis. Hence, their possible universal property should be investigated. A similar interpretation can be drawn on the values of $t_{0,d}$ reported above. A question might arise concerning the capability of each fluctuation measure to localize and detect how the correlation evolves along the growth of

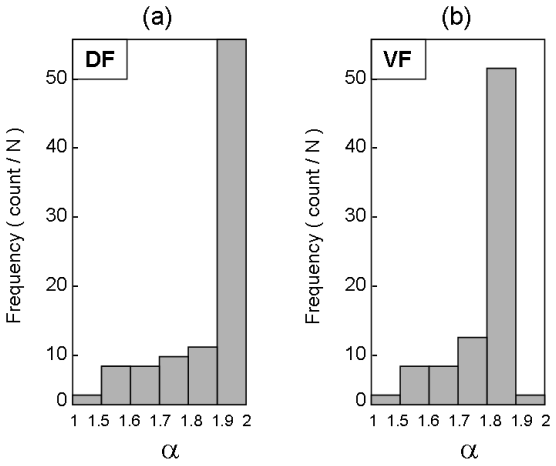

Fig. 7: Histograms for the scaling exponents α: DF (a) and VF (b).

fingering patterns. Our results have shown that the mixing length has no sensitivity in detecting the expected correlation relaxation due to the stabilization of the nonlinear regime. However, as shown in fig. 6(b), the DFA scaling exponent works as a high sensitive probe for that. Indeed, we believe this is a remarkable property allowing more accurate fingering characterization and modeling validation when facing results from real experiments.

In summary, the present fluctuation analysis strongly supports the signature of the underlying density or viscosity process on the fingering pattern formation. Taking into account our results, one can say that DF and VF fingering patterns are indeed slightly different. More precisely, at least for the canonical case $R = R_a = 3$, DFA allows to have complementary information to those obtained just from mixing length. The behavior of α, computed on transversely averaged concentration profiles, is a new diagnostic for the structural correlation evolution due to processes like spreading, shielding or splitting of fingers in fluid interfaces. In particular, DFA provides therefore a new complementary measure in the study of fingering dynamics, characterizing the instantaneous self-affinity of the fingering pattern throughout the evolution of concentration averaged profiles. A major challenge we are currently considering in using DFA to characterize fingering pattern formation is the comparison of $\langle c(x,t)\rangle$ fluctuation between fingering simulation and some experimental observations in miscible displacements. Such a procedure will allow for either a validation of the fingering mechanism and provide insights into where and which types of system modifications affect the fingering pattern formation. Finally, a complementary study which does include more sensitive measures, as those from the so-called gradient pattern analysis [20–22], is currently in progress.

* * *

The authors acknowledge financial support from the Brazilian agency CNPq (Grants 1173/2005-0, 0524/2007-0, 141173/2005-0, 200524/2007-0), Belgian Prodex, FNRS, Université Libre de Bruxelles (ULB) and the Communauté Française de Belgique (ARC programme). We thank M. Mishra, A. F. da Silva, H. F. Campos Velho and J. Pontes for fruitful discussions.

REFERENCES

[1] Wesfreid J. E., Brand H. R., Manneville P., Albinet G. and Boccara N., *Propagation in Systems far from Equilibrium* (Springer, Berlin) 1984.
[2] Pontes J., Walgraef D. and Christov C. I., *J. Comput. Interdiscip. Sci.*, **1** (2008) 11.
[3] Hill S., *Chem. Eng. Sci.*, **1** (1952) 247.
[4] Tan C. T. and Homsy G. M., *Phys. Fluids*, **29** (1986) 3549.
[5] Homsy G. M., *Annu. Rev. Fluid Mech.*, **19** (1987) 271.
[6] Tan C. T. and Homsy G. M., *Phys. Fluids*, **31** (1988) 1330.
[7] Zimmerman W. B. and Homsy G. M., *Phys. Fluids A*, **3** (1991) 1859.
[8] Manickam O. and Homsy G. M., *J. Fluid Mech.*, **288** (1995) 75.
[9] Fernandez J., Kurowski P., Petitjeans P. and Meiburg E., *J. Fluid Mech.*, **451** (2002) 239.
[10] Trevelyan P. M. J., Almarcha C. and De Wit A., to be published in *J. Fluid Mech.* (2010).
[11] Hu K., Ivanov P. C., Chen Z., Carpena P. and Stanley H. G., *Phys. Rev. E*, **64** (2001) 011114.
[12] D'Hernoncourt J., Zebib A. and De Wit A., *J. Fluid Mech.*, **576** (2007) 445; *ibid Phys. Rev. Lett.*, **96** (2006) 154501.
[13] Tchelepi H. A., Orr F. M. jr., Rakotomalala N., Salin D. and Woumeni R., *Phys. Fluids A*, **5** (1993) 1558.
[14] Peng C.-K., Buldyrev S. V., Havlin S., Simons M., Stanley H. E. and Goldberger A. L., *Phys. Rev. E*, **49** (1994) 1685.
[15] Bunde A. *et al.*, *Phys. Rev. E*, **85** (2000) 3736.
[16] Buldyrev S. V., Goldberger A. L., Havlin S., Mantegna R. N., Matsa C. K. and Peng C.-K. *et al.*, *Phys. Rev. E*, **51** (1995) 5084.
[17] Bai M. Y. and Zhu H. B., *Physica A*, **389** (2010) 1883.
[18] Moret M. A., Zebende G. F., Nogueira E. and Pereira M. G., *Phys. Rev. E*, **68** (2003) 041104.
[19] Rosa R. R., Ramos F. M., Caretta C. A. and Campos Velho H. F., *Comput. Phys. Commun.*, **180** (2009) 621.
[20] Rosa R. R., Sharma A. S. and Valdivia J. A., *Int. J. Mod. Phys. C*, **10** (1999) 147.
[21] Ferreira da Silva A. *et al.*, *Solid State Commun.*, **113** (2000) 703.
[22] Baroni M. P. M. A. *et al.*, *Microelectron. J.*, **37** (2006) 290.